Advances in Continuous and Discrete Models

RESEARCH Open Access

The propagation dynamics of UAU-SEPIR in two-layered networks

Li Yan[1*] and Zhen Han[2]

*Correspondence:
Yanlinpu_2016@163.com
[1]School of Computer Science, Northwestern Polytechnical University, Xi'an, 710072, Shaanxi, P.R. China
Full list of author information is available at the end of the article

Abstract

The frequent emergence of new infectious diseases poses a serious threat to human health and social development. In the current digital age, the widespread application of online social networks has accelerated the dissemination of information regarding these diseases, influencing the interplay between disease spread and information diffusion. To address this, we propose the *UAU–SEPIR* model, a novel two-layered network propagation model inspired by the early stages of the COVID-19 outbreak. This model, constructed using a micro-Markov-chain approach, features an upper layer for information diffusion (the *UAU* model) and a lower layer for disease propagation (the *SEPIR* model). We derive the epidemic threshold, which is influenced by the dynamics of information diffusion, the network topology of disease spread, and the pathways from exposed to infected to recovered individuals. Through extensive random simulations, we confirmed the validity of our model. The research findings reveal that both model parameters and network topology play crucial roles in shaping the interaction between information diffusion and disease spread. Additionally, in random networks, adaptive behavior of individuals significantly enhances the inhibition of disease transmission. Overall, Our study provides theoretical insights into the interplay between social-network dynamics and the early outbreak stages, offering valuable support for disease prevention and control strategies.

Keywords: Two-layered network; Disease spread; Information diffusion; Epidemic threshold

1 Introduction

Throughout human history, infectious diseases have been a persistent threat. The COVID-19 pandemic, which began in late 2019, has persisted for over four years. It is the most impactful and widespread infectious disease of the 21st century, causing unprecedented disruptions to daily life and significant socioeconomic consequences [1–6]. Despite the ongoing effects of COVID-19, the emergence of the monkeypox outbreak in 2024 introduces new challenges, further extending the era of global health crises and underscoring that the threat of infectious diseases remains ever-present [7–10].

Increasingly, scholars in the public-health field recognize dynamic models as powerful tools for studying the spread and outbreak of infectious diseases. Since Kermack and

McKendrick first introduced the compartmental model for studying infectious diseases in 1927 [11], an increasing number of researchers have developed various models based on this framework. These models aim to analyze the mechanisms of disease spread and to predict future trends in disease development. Typically, these models assume a uniformly mixed population, where each individual has an equal probability of being exposed to others within a given time frame. However, in reality, contact frequency and the disease status of individuals vary significantly. To address this, incorporating individual differences in contact frequency is crucial. Consequently, simulating contact patterns through complex networks has emerged as an effective method, making the study of infectious-disease spread through these networks a major research direction [12–20].

In reality, the spread of infectious diseases involves both the disease itself and the diffusion of related information. Such information is commonly shared through online social networks like Weibo, WeChat, Twitter (X), and Facebook [21–26]. Upon receiving information about a disease, individuals often adopt preventive measures, such as improving personal hygiene, limiting public-place visits, and maintaining social distancing. Additionally, infected individuals may actively share information on these platforms. Thus, the diffusion of disease-related information can influence disease spread, and conversely, disease spread can impact information diffusion.

The traditional single-layer network model is limited in capturing the interaction between infectious-disease spread and information diffusion. To more accurately represent the complexity of disease spread, constructing a multilayer network topology structure is essential [27–37]. Bauch and Galvani investigated the coupling effect between information diffusion and disease spread in such networks [27]. Granell et al. developed a *UAU*–*SIS* model using a micro-Markov-chain approach to describe how epidemic transmission and awareness diffusion interact within multilayer networks. They discovered that the epidemic threshold depends not only on the disease layer's network topology, but also on the information layer's diffusion dynamics [28]. Zheng et al. introduced the *UAU*–*SIR* models to account for the cases where recovered individuals are not reinfected [29]. Guo et al. constructed a *UAU*–*SIS* two-layered network model incorporating local influence effects, revealing two-stage changes in epidemic threshold influenced by local awareness [31]. Wang et al. utilized micro-Markov chains to establish a *UAU*–*SIR* two-layer network model, and then analyzed how the epidemic threshold is influenced by both information-diffusion and disease-layer topology [32]. David et al. studied how the overlap ratio between the information and disease layers affects the final epidemic size [34]. Ye et al. proposed a heterogeneous propagation model of disease-behavior nformation to explore the effect of individual risk perception and behavioral differences on disease spread [35].

However, in the above related works, traditional infectious disease models like SIS, SIR, and SEIR are commonly used. To better understand real-world scenarios and devise more effective prevention and control strategies, we focus on the early stages of the COVID-19 outbreak when no control measures were in place [38]. We modeled this scenario using a UAU (Unaware-Aware-Unaware) information diffusion model and SEPIR (Susceptible-Exposed-Presymptomatic-Infectious-Recovered) disease model with a two-layered network. This approach allow us to delve into how interactions between the information and disease layers impact epidemic threshold and propagation dynamics.

The structure of this paper is organized as follows: Sect. 2 introduces a *UAU*–*SEPIR* two-layered network propagation model, which combines the UAU model for information

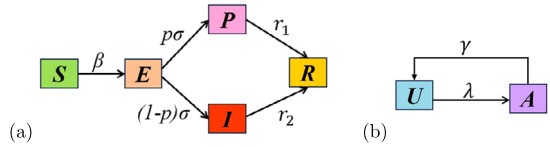

Figure 1 (a) The transition process of infectious-disease states, (b) The transition process of information states

diffusion with the SEPIR model for disease dynamics, based on the micro-Markov-chain framework; Sect. 3 analyzes the epidemic threshold; Sect. 4 presents a comparison between numerical simulations and random simulations, demonstrating the consistency of the fitting results, and then discusses key numerical findings; Sect. 5 provides a summary of the conclusions and discussions.

2 Model formation

During the COVID-19 pandemic [38], the research population can be categorized into five different groups according to the disease states: susceptible or healthy group (S), exposed group (E), infectious but not yet symptomatic group (P), symptomatic infected group (I) and recovered group (R). The birth and death rates of the population are considered negligible in this model. Within a unit of time, susceptible individuals come into contact with infected individuals and become exposed at a rate of β. Among the exposed individuals, a proportion of p transition to the presymptomatic group at a rate of σ, while the remaining proportion of $1-p$ transition to the symptomatic infected group at the same rate of σ. The presymptomatic individuals recover at a rate of r_1, and the symptomatic infected individuals enter the recovered group with a rate of r_2. The transition dynamic of the disease states is illustrated in Fig. 1(a).

At the same time, information about infectious diseases is often disseminated through virtual social platforms, which can influence disease transmission in the real world. For instance, healthy individuals may adopt self-protection measures in response to such information, thereby reducing their infection risk. We categorize the same population into two groups based on their awareness of the disease: the unaware group (U) and the aware group (A). Unaware individuals transition to the aware group at a rate of λ through information exchange with aware individuals. Aware individuals may revert to the unaware group at a rate of γ due to forgetting or information fatigue. The transition dynamic of the information states is illustrated in Fig. 1(b).

We use a two-layered network to simulate the spread of both diseases and information within the same population. The network consists of:

(1) *Online Social Network (Layer 1):* This layer models the dissemination of information related to infectious diseases based on the *UAU* propagation model. In this network, nodes represent individuals, and edges represent the transmission of information between them.

(2) *Physical Social Network (Layer 2):* This layer represents actual physical contacts among individuals, simulating the spread of infectious diseases, based on the *SEPIR* model. Here, edges represent friendship relationships, which facilitate the physical transmission of diseases.

We assume that each node in the two layers corresponds to the same individual, although the network topologies of the two layers can differ. Figure 2 shows the architecture of this two-layered network, where each individual has two simultaneous states: a disease

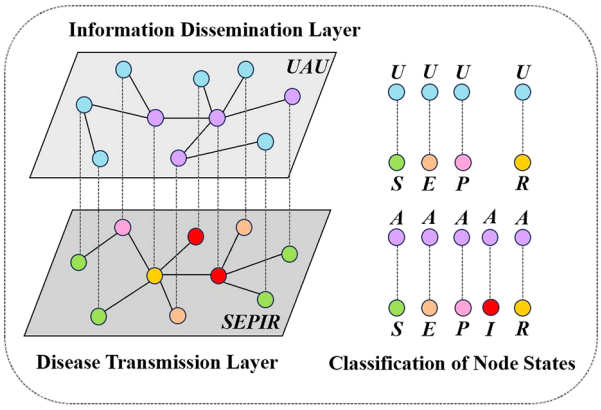

Figure 2 Schematic diagram of the two-layered network and the classification of node states: the upper layer represents the information-dissemination network; The lower layer represents the disease-spread network

state and an information state. Consequently, the population is categorized into *US*, *AS*, *UE*, *AE*, *UP*, *AP*, *AI*, *UR*, *AR* states, as depicted in Fig. 2. In the upper and lower layers of the network, let the number of nodes be N and they are both undirected graphs. The adjacency matrix of the upper layer network is $A = (a_{ij})_{N\times N}$, where $a_{ij} = 1$ indicates that there is an edge between node i and node j, otherwise $a_{ij} = 0$. The adjacency matrix of the lower layer network is $B = (b_{ij})_{N\times N}$, where $b_{ij} = 1$ indicates that there is an edge between node i and node j, otherwise $b_{ij} = 0$. Actually, the dynamics in one layer (information dissemination) influence the dynamics in the other layer (disease transmission). The susceptible individuals with awareness (*AS*) reduce their risk of infection by adjusting their behavior (such as reducing access to public places, maintaining social distancing, etc.), resulting in a lower infection rate coefficient β_A than the β of susceptible individuals with unawareness, i.e., $\beta_A = \delta\beta$. The exposed individuals with unawareness (*UE*) will transition directly to the aware and infected individuals (*AI*). This transition occurs because these individuals become aware of the disease after experiencing relevant symptoms. Consequently, we do not include the unaware and infected state (*UA*) in the model, as shown in Fig. 2.

For the needs of subsequent modeling, we define $\lambda_i(t)$ as the probability that node i does not communicate disease-related information with any neighboring nodes in the information layer, expressed as:

$$\lambda_i(t) = \prod_j (1 - \lambda a_{ij} p_j^A(t)), \tag{1}$$

where the symbol $\prod$ denotes a product over multiple terms, $p_j^A(t)$ represents the probability that node j is an aware individual at time t. Defining T_i^U as the probability of an unaware and susceptible individual being infected by the infected neighbors in the disease layer, then:

$$T_i^U(t) = \prod_j (1 - \beta b_{ij} p_j^{AI}(t)), \tag{2}$$

where $p_j^{AI}(t)$ represents the probability that node j is an aware and infected individual at time t. Similarly, T_i^A represents the probability of an aware and susceptible individual

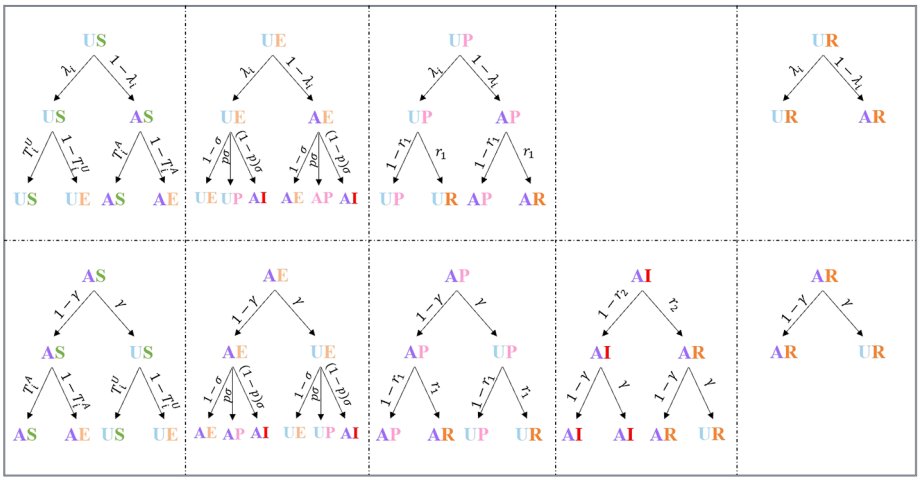

Figure 3 Schematic diagram of probability-transition tree for nine states (*US*, *UE*, *UP*, *UR*, *AS*, *AE*, *AP*, *AI*, and *AR*). Each state can transition to other states based on specific probabilities, illustrated by arrows and formulas on the branch lines. The diagram ensures that the sum of probabilities for all possible transitions from any given state equals 1

being infected by infected neighbors, then:

$$T_i^A(t) = \prod_j (1 - \delta\beta b_{ij} p_j^{AI}(t)). \tag{3}$$

In the two-layered network model *UAU*–*SEPIR*, nodes can be in one of nine states: *US*, *AS*, *UE*, *AE*, *UP*, *AP*, *AI*, *UR*, *AR*. Each state transitions to other states based on a specific probability, forming a state-transition probability tree, as in Fig. 3. For states other than *UR* and *AR* states, transitions involve changes in both the information layer and the disease layer. For example, in the *US* state, the first layer determines whether a node remains unaware or transitions to the aware state. With probability λ_i, the node stays in the *US* state, while with probability $1 - \lambda_i$, it moves to the *AS* state. In the second layer, if a node in the *US* state is not infected with probability T_i^U, it remains in *US*; otherwise, it transitions to *UE* with probability $1 - T_i^U$. Similarly, for the *AS* state, the uninfected probabilities are adjusted to T_i^A for remaining in *AS* and $1 - T_i^A$ for transitioning to *AE*.

For nodes in the *UE* and *AE* states, transitions can be categorized into three scenarios: 1) With probability $1 - \sigma$, the node stays in the same state (*UE* or *AE*); 2) With probability $p\sigma$, the node transitions to the presymptomatic state (*UP* or *AP*); 3) With probability $(1 - p)\sigma$, it moves to the symptomatic infected state (*AI*). For the *UR* and *AR* states, transitions only involve changes in the information layer: in the *UR* state, with probability λ_i, the node remains in *UR*, and with probability $1 - \lambda_i$, it transitions to *AR*. Similarly, in the *AR* state, the node either stays in *AR* with probability $1 - \gamma$ or transitions back to *UR* with probability γ. This diagram ensures that the sum of probabilities for all possible transitions from any given state equals 1.

Defining p_i^{US}, p_i^{AS}, p_i^{UE}, p_i^{AE}, p_i^{UP}, p_i^{AP}, p_i^{AI}, p_i^{UR}, p_i^{AR} as the probability that node i is in states *US*, *AS*, *UE*, *AE*, *UP*, *AP*, *AI*, *UR*, *AR* at time t, and based on the state-transition probability tree depicted in Fig. 3, the following dynamic model is constructed using the

micro-Markov-chain method:

$$\begin{cases} p_i^{US}(t+1) = p_i^{US}(t)\lambda_i(t)T_i^U(t) + p_i^{AS}(t)\gamma T_i^U(t), \\ p_i^{AS}(t+1) = p_i^{US}(t)(1-\lambda_i(t))T_i^A(t) + p_i^{AS}(t)(1-\gamma)T_i^A(t), \\ p_i^{UE}(t+1) = p_i^{US}(t)\lambda_i(t)(1-T_i^U(t)) + p_i^{AS}(t)\gamma(1-T_i^U(t)) \\ \qquad\qquad +p_i^{UE}(t)\lambda_i(t)(1-\sigma) + p_i^{AE}(t)\gamma(1-\sigma), \\ p_i^{AE}(t+1) = p_i^{US}(t)(1-\lambda_i(t))(1-T_i^A(t)) + p_i^{AS}(t)(1-\gamma)(1-T_i^A(t)) \\ \qquad\qquad +p_i^{UE}(t)(1-\lambda_i(t))(1-\sigma) + p_i^{AE}(t)(1-\gamma)(1-\sigma), \\ p_i^{UP}(t+1) = p_i^{UE}(t)\lambda_i(t)p\sigma + p_i^{AE}(t)\gamma p\sigma + p_i^{UP}(t)\lambda_i(t)(1-r_1) \\ \qquad\qquad +p_i^{AP}(t)\gamma(1-r_1), \\ p_i^{AP}(t+1) = p_i^{UE}(t)(1-\lambda_i(t))p\sigma + p_i^{AE}(t)(1-\gamma)p\sigma \\ \qquad\qquad +p_i^{UP}(t)(1-\lambda_i(t))(1-r_1) + p_i^{AP}(t)(1-\gamma)(1-r_1), \\ p_i^{AI}(t+1) = p_i^{UE}(t)(1-p)\sigma + p_i^{AE}(t)(1-p)\sigma + p_i^{AI}(t)(1-r_2), \\ p_i^{UR}(t+1) = p_i^{UP}(t)\lambda_i(t)r_1 + p_i^{AP}(t)\gamma r_1 + p_i^{AI}(t)\gamma r_2 + p_i^{UR}(t)\lambda_i(t) + p_i^{AR}(t)\gamma, \\ p_i^{AR}(t+1) = p_i^{UP}(t)(1-\lambda_i(t))r_1 + p_i^{AP}(t)(1-\gamma)r_1 + p_i^{AI}(t)(1-\gamma)r_2 \\ \qquad\qquad +p_i^{UR}(t)(1-\lambda_i(t)) + p_i^{AR}(t)(1-\gamma). \end{cases} \tag{4}$$

System (4) tracks the evolution of node probabilities over time by considering the state transitions detailed in Fig. 3, with each transition governed by the probabilities specified in the state-transition tree.

At any time t, the sum of the probabilities of any given node i in the two-layered network being in these nine states is 1, that is:

$$p_i^{US}(t) + p_i^{AS}(t) + p_i^{UE}(t) + p_i^{AE}(t) + p_i^{UP}(t) + p_i^{AP}(t) + p_i^{AI}(t) + p_i^{UR}(t) + p_i^{AR}(t) = 1. \tag{5}$$

When $t \to +\infty$, system (4) reaches steady state $E^* = (p_i^{US*}, p_i^{AS*}, p_i^{UE*}, p_i^{AE*}, p_i^{UP*}, p_i^{AP*}, p_i^{AI*}, p_i^{UR*}, p_i^{AR*})$, satisfying

$$\begin{cases} p_i^{US}(t+1) = p_i^{US}(t) = p_i^{US*}, (t \to \infty), \\ p_i^{AS}(t+1) = p_i^{AS}(t) = p_i^{AS*}, (t \to \infty), \\ p_i^{UE}(t+1) = p_i^{UE}(t) = p_i^{UE*}, (t \to \infty), \\ p_i^{AE}(t+1) = p_i^{AE}(t) = p_i^{AE*}, (t \to \infty), \\ p_i^{UP}(t+1) = p_i^{UP}(t) = p_i^{UP*}, (t \to \infty), \\ p_i^{AP}(t+1) = p_i^{AP}(t) = p_i^{AP*}, (t \to \infty), \\ p_i^{AI}(t+1) = p_i^{AI}(t) = p_i^{AI*}, (t \to \infty), \\ p_i^{UR}(t+1) = p_i^{UR}(t) = p_i^{UR*}, (t \to \infty), \\ p_i^{AR}(t+1) = p_i^{AR}(t) = p_i^{AR*}, (t \to \infty) \end{cases} \tag{6}$$

and the following expression

$$p_i^{US*} + p_i^{AS*} + p_i^{UE*} + p_i^{AE*} + p_i^{UP*} + p_i^{AP*} + p_i^{AI*} + p_i^{UR*} + p_i^{AR*} = 1.$$

3 The epidemic threshold

The epidemic threshold β_c is a key indicator for determining the potential for an infectious-disease outbreak. If the infection rate β exceeds this threshold β_c, the disease is likely to persist within the population. Conversely, if β is below β_c, the disease is expected to rapidly decline, and the epidemic is likely to end relatively quickly.

Let $\xi_i = p_i^{AI*}$, and when the infection rate of the disease layer approaches the epidemic threshold, we assume $\xi_i \ll 1$. Based on this assumption, we can further derive:

$$T_i^{UI}(t) \approx 1 - \alpha_i^{UI},\ T_i^{A}(t) \approx 1 - \alpha_i^{A},$$

where $\alpha_i^A = \delta\beta \sum_j b_{ij}\xi_j$, $\alpha_i^{UI} = \beta \sum_j b_{ij}\xi_j$. In this case, the first four equations of system (4) can be transformed as:

$$\begin{cases} p_i^{US}(t+1) = p_i^{US}(t)\lambda_i(t)(1-\alpha_i^{UI}) + p_i^{AS}(t)\gamma(1-\alpha_i^{UI}), \\ p_i^{AS}(t+1) = p_i^{US}(t)(1-\lambda_i(t))(1-\alpha_i^{A}) + p_i^{AS}(t)(1-\gamma)(1-\alpha_i^{A}), \\ p_i^{UE}(t+1) = p_i^{US}(t)\lambda_i(t)\alpha_i^{UI} + p_i^{AS}(t)\gamma\alpha_i^{UI} + p_i^{UE}(t)\lambda_i(t)(1-\sigma) \\ \qquad\qquad + p_i^{AE}(t)\gamma(1-\sigma), \\ p_i^{AE}(t+1) = p_i^{US}(t)(1-\lambda_i(t))\alpha_i^{A} + p_i^{AS}(t)(1-\gamma)\alpha_i^{A} \\ \qquad\qquad + p_i^{UE}(t)(1-\lambda_i(t))(1-\sigma) + p_i^{AE}(t)(1-\gamma)(1-\sigma). \end{cases} \tag{7}$$

Since the remaining five equations in system (4) maintain their original form in this case, they will not be repeated here.

When the above system (7) is in a steady state and the number of infected individuals is very small, we can assume that $p_i^{UIP*} \to 0$, $p_i^{AP*} \to 0$, $p_i^{UIR*} \to 0$, $p_i^{AR*} \to 0$. Then, the equations related to p_i^{UP}, p_i^{AP}, p_i^{UR} p_i^{AR} can be ignored. Consequently, we focus only on the first four key equations and equation ξ_i in system (7). By further neglecting the higher-order nonlinear terms in these equations, we derive the following steady-state system:

$$\begin{cases} p_i^{US*} = p_i^{US*}\lambda_i + p_i^{AS*}\gamma, \\ p_i^{AS*} = p_i^{US*}(1-\lambda_i) + p_i^{AS*}(1-\gamma), \\ p_i^{UE*} = p_i^{US*}\lambda_i\alpha_i^{UI*} + p_i^{AS*}\gamma\alpha_i^{UI*} + p_i^{UE*}\lambda_i(1-\sigma) + p_i^{AE*}\gamma(1-\sigma), \\ p_i^{AE*} = p_i^{US*}(1-\lambda_i)\alpha_i^{A*} + p_i^{AS*}(1-\gamma)\alpha_i^{A*} + p_i^{UE*}(1-\lambda_i)(1-\sigma) \\ \qquad + p_i^{AE*}(1-\gamma)(1-\sigma), \\ \xi_i = (p_i^{UE*} + p_i^{AE*})\sigma(1-p) + \xi_i(1-r_2). \end{cases} \tag{8}$$

From the above system (8), we can calculate:

$$\sigma(p_i^{UE*} + p_i^{AE*}) = \alpha_i^{UI} p_i^{US*} + \alpha_i^{A} p_i^{AS*}. \tag{9}$$

By substituting equation (9) into ξ_i in system (8), we can derive:

$$\xi_i = \xi_i(1-r_2) + (1-p)(p_i^{US*} + \delta p_i^{AS*})\beta \sum_j b_{ji}\xi_j. \tag{10}$$

The probability of any given node i being in an aware state is:

$$p_i^{A*} = p_i^{AS*} + p_i^{AI*} + p_i^{AP*} + p_i^{AR*},$$

then we can obtain $p_i^{A*} \approx p_i^{AS*}$. we further derive $p_i^{US*} \approx 1 - p_i^{A*}$. Thus, we can derive the following equation:

$$\frac{r_2}{1-p}\xi_i = (1 - p_i^{A*} + \delta p_i^{A*})\beta \sum_j b_{ij}\xi_j, \tag{11}$$

through further organization, we can obtain:

$$\sum_j [(1 - (1-\delta)p_i^{A*})b_{ji} - \frac{r_2}{\beta(1-p)}t_{ij}]\xi_j = 0. \tag{12}$$

Let $c_{ij} = (1 - (1-\delta)p_i^{A*})b_{ij}$, depending on the adjacency matrix element b_{ij} of the disease layer and the probability p_i^{A*} that node i is an aware individual at steady state. As i and j vary from 1 to N, c_{ij} forms a matrix $C = (c_{ij})_{N\times N}$. From equation (12), we can derive the expression for the epidemic threshold:

$$\beta_c = \frac{r_2}{(1-p)\Lambda_{max}(C)}, \tag{13}$$

where $\Lambda_{max}(C)$ represents the maximum eigenvalue of matrix $C = (c_{ij})_{N\times N}$. Obviously, the epidemic threshold β_c^U is influenced by both the network structure of the disease layer and the propagation dynamics of the information layer. Furthermore, β_c is affected by the proportion $1-p$ of the exposed individuals who transition to the infected state, as well as the rate r_2 at which infected individuals recover. This suggests that β_c depends significantly on the transmission pathway $E \to I \to R$, likely due to the fact that the source of infection is the infected individuals I.

4 Simulation results

In this section, we use a configuration model to generate two-layered networks with N nodes, constructing four distinct network structures: 1) SF-SF network, where the upper layer is a scale-free network with $p(k) \sim k^{-3}$, and the lower layer is also a scale-free network with $p(k) \sim k^{-2.5}$; 2) R-R network, where the upper layer is a random network with $\langle k\rangle = 10$, and the lower layer is a random network with $\langle k\rangle = 6$; 3) SF-R network, where the upper layer is a scale-free network with $p(k) \sim k^{-3}$, and the lower layer is a random network with $\langle k\rangle = 6$; 4) R-SF network, where the upper layer is a random network with $\langle k\rangle = 10$, nd the lower layer is also a scale-free network with $p(k) \sim k^{-2.5}$. Using the state-transition probability tree depicted in Fig. 3, we employ the Monte Carlo simulation method to model disease and information propagation across these two-layered networks [28]. The numerical simulation are based on system (4). In practice, the focus is on the densities of various disease states – denoted as $\rho^S(t)$, $\rho^E(t)$, $\rho^P(t)$, $\rho^I(t)$, $\rho^R(t)$ – with particular attention to asymptomatic and symptomatic infected individuals. Similarly, for information dissemination, we track the density of different information states, denoted as $\rho^U(t)$, $\rho^A(t)$. The calculation formulas for the densities of various disease states and

information states during the simulation process are:

$$\rho^S(t) = \frac{\sum_{i=1}^{N}(p_i^{US}(t) + p_i^{AS}(t))}{N},\ \rho^E(t) = \frac{\sum_{i=1}^{N}(p_i^{UE}(t) + p_i^{AE}(t))}{N}, \rho^I(t) = \frac{\sum_{i=1}^{N} p_i^{AS}(t)}{N},$$

$$\rho^P(t) = \frac{\sum_{i=1}^{N}(p_i^{UP}(t) + p_i^{AP}(t))}{N},\ \rho^R(t) = \frac{\sum_{i=1}^{N}(p_i^{UR}(t) + p_i^{AR}(t))}{N},$$

$$\rho^U(t) = \frac{\sum_{i=1}^{N}(p_i^{US}(t) + p_i^{UE}(t) + p_i^{UP}(t) + p_i^{UR}(t))}{N},$$

$$\rho^A(t) = \frac{\sum_{i=1}^{N}(p_i^{AS}(t) + p_i^{AE}(t) + p_i^{AP}(t) + p_i^{AI}(t) + p_i^{AR}(t))}{N}.$$

Consequently, this section focuses on illustrating the temporal changes in these densities. In the following work, we will use $N = 1000$, $\lambda = 0.28$, $\gamma = 0.3$, $\beta = 0.24$, $\delta = 0.2$, $\sigma = 1/7$, $p = 0.2$, $r_1 = 0.14$, and $r_2 = 0.33$ as the benchmark parameters for the relevant simulations.

To validate model (4), we compare its numerical solution (black curve) with results from 50 independent Monte Carlo simulations (brown circles). Figure 4 clearly shows that the numerical results align well with the Monte Carlo simulations. Figure 4 also depicts the density changes of various coupling states. ρ^{US} decreases rapidly initially, then more slowly, approaching a nonzero steady-state value. ρ^{UE} and ρ^{UP} rise to a high peak before declining to zero. ρ^{UR} increases rapidly at first, then stabilizes at a steady-state value. ρ^{AS} also increases rapidly, then decreases and stabilizes at a steady-state value. The initial increase in ρ^{AS} is due to U in the US state becoming an aware individual, resulting in an increase in AS. The ρ^{AE}, ρ^{AP}, and ρ^{AI} show trends similar to ρ^{UE} and ρ^{UP}, reflecting the typical disease stages of susceptible individuals through stages E, P, or I before reaching R, hence the densities tend to zero. ρ^{AR} rises quickly before stabilizing at a steady-state value. Additionally, Fig. 12 in Appendix A shows the density changes of these coupled states in the R-R network, the numerical results align well with the random simulation results. This consistency suggests that the outcomes of the numerical and random simulation methods are not influenced by the network structure.

To investigate the impact of the coupling changes between the information-diffusion rate λ and network topology on spreading behaviors, we examined different λ values across the four network structures in Fig. 5. The first, second, third, and fourth rows correspond to the SF-SF, R-R, SF-R, and R-SF networks, respectively. Overall, increasing λ promotes the information diffusion while suppressing epidemic spread. This suggests that an increase in aware individuals, due to a higher λ, leads to more aware and susceptible individuals, thereby reducing the disease transmission rate and mitigating the prevalence of diseases. For the SF-SF network and SF-R network, the information layer's propagation accelerates significantly as λ increases from 0.2 to 0.5, with diminishing effects beyond 0.5. In contrast, when the upper layer is a random network, λ changes have minimal impact on information propagation, indicating that random networks' structural heterogeneity diminishes the influence of the information-propagation rate. Conversely, scale-free networks show a more pronounced impact, where increased λ has a notable effect on information diffusion. A similar trend is observed in the disease layer, but with sensitivity to

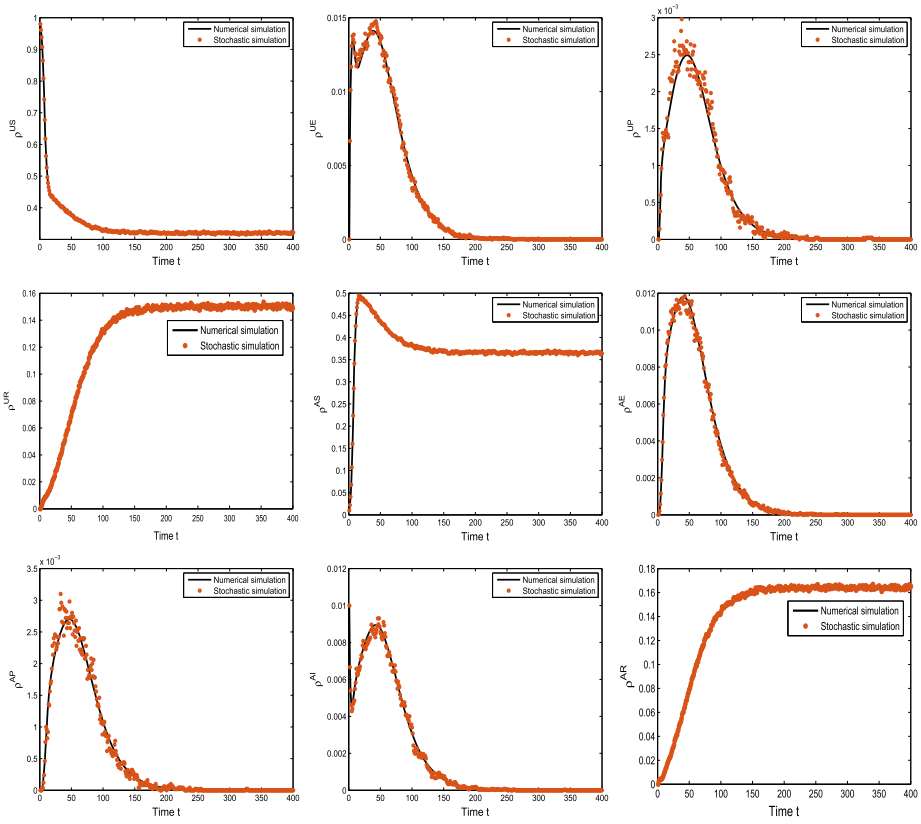

Figure 4 The time evolutions of ρ^{US}, ρ^{AS}, ρ^{UE}, ρ^{AE}, ρ^{UP}, ρ^{AP}, ρ^{AI}, ρ^{UR}, ρ^{AR} in the SF-SF network, where both layers of the network are scale-free. The black curves represent the results from numerical simulations of system (4), while the brown circles indicate the average values obtained from 50 random simulations

network structure varying as follows: SF-SF network > R-R network > SF-R network > R-SF network. These results demonstrate that the epidemic spread is more sensitive to network structure changes.

Figure 6 illustrates the impact of the transmission rate β and network structure on the time evolutions of ρ^S, ρ^I, ρ^R, ρ^U, ρ^A. β has almost no impact on information diffusion (see the last two columns), consistent with our modeling expectations. However, β significantly affects the epidemic spread. Specifically, an increase in β advances the high peak arrival time of the infectious disease, raises the high peak value, and enlarges the final epidemic size. This effect is particularly pronounced when β increases from 0.2 to 0.5. The final epidemic size, ordered by network structure, is R-SF < SF-SF < R-R < SF-R, suggesting that the scale-free network structure in the disease layer tends to reduce the overall epidemic size.

Figure 7 shows the influence of forgetting rate γ of aware individuals and network structure on the time evolutions of ρ^S, ρ^I, ρ^R, ρ^U, ρ^A. As γ increases, the diffusion of information is notably suppressed. The final values of ρ^U and ρ^A are almost identical in both the SF-SF and SF-R networks. In contrast, for the R-R and R-SF networks, the evolution trends of ρ^U and ρ^A are similar. This suggests that scale-free networks exhibit a more pronounced suppression effect on information diffusion compared to random networks, making them less conducive to the spread of information. However, as γ increases, the

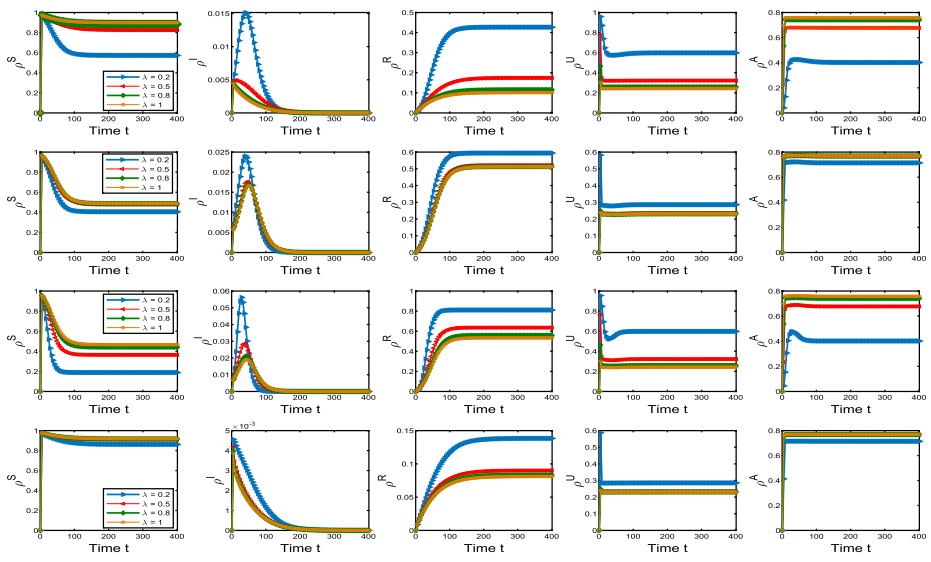

Figure 5 The time evolutions of ρ^S, ρ^I, ρ^R, ρ^U, ρ^A are illustrated for the four different network structures, with varying information-diffusion rates $\boldsymbol{\lambda}$. The first, second, third, and fourth rows correspond to the SF-SF network, R-R network, SF-R network, and R-SF network, respectively

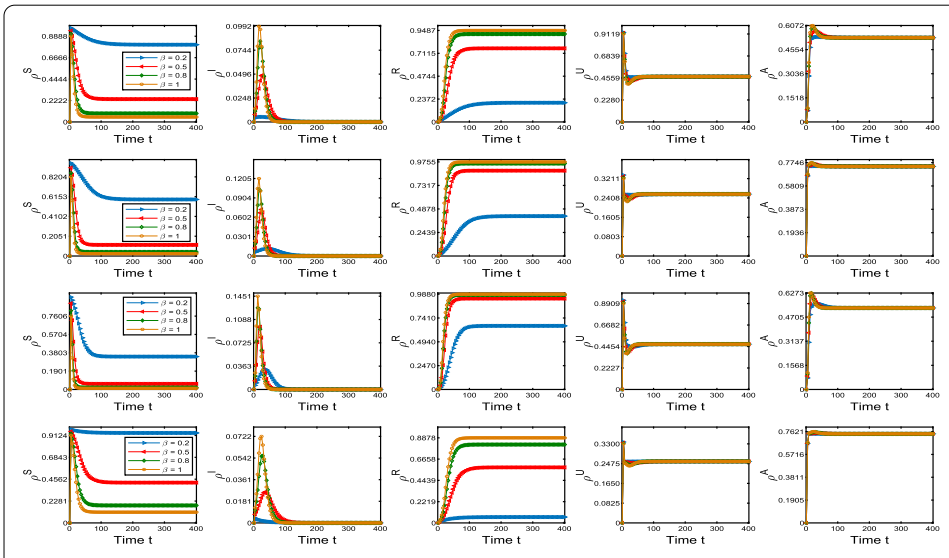

Figure 6 The time evolutions of ρ^S, ρ^I, ρ^R, ρ^U, ρ^A are illustrated for the four different network structures, with varying transmission rates $\boldsymbol{\beta}$. The first, second, third, and fourth rows correspond to the SF-SF network, R-R network, SF-R network, and R-SF network, respectively

spread of the disease layer is promoted. With fewer aware and susceptible individuals, the transmission rate is β, resulting in a higher peak infection rate. Consequently, the final epidemic sizes follow the order of network structure: R-SF <SF-SF<R-R<SF-R (see the third columns). This indicates that scale-free networks have a less pronounced effect on promoting disease spread compared to random networks.

Figure 8 displays the effect of the transmission-rate ratio, δ, on disease spread in a SF-SF network. As δ increase, ρ^S decreases, the high peak values of ρ^E, ρ^P, ρ^I become large, and

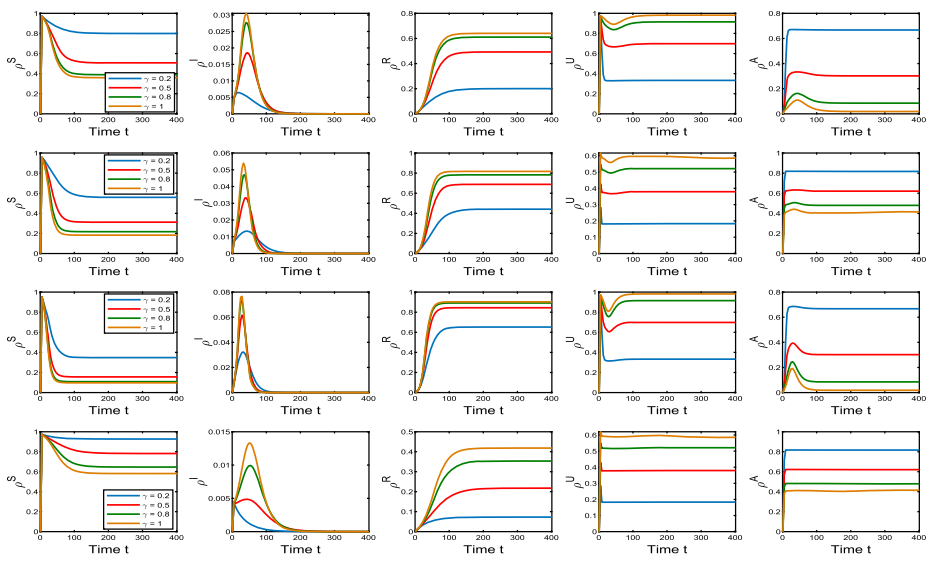

Figure 7 The time evolutions of ρ^S, ρ^I, ρ^R, ρ^U, ρ^A are illustrated for the four different network structures, with varying transmission rates γ. The first, second, third, and fourth rows correspond to the SF-SF network, R-R network, SF-R network, and R-SF network, respectively

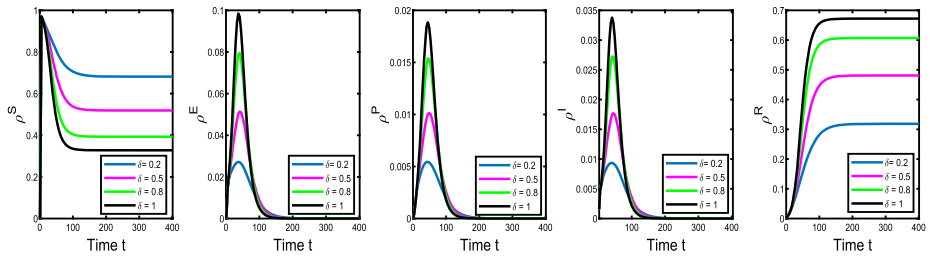

Figure 8 With different ratio of transmission rates δ, the time evolutions of ρ^S, ρ^E, ρ^P, ρ^I, ρ^R on the SF-SF network

ρ^R increases. Overall, a higher δ accelerates the spread of the disease and results in a larger final epidemic size.

The impact of transition proportion p on disease spread is displayed in Fig. 9. We can observe that when p becomes large, the rate of decrease in ρ^S slows, and its steady-state value increases, and then the steady-state value of ρ^R decreases. However, the high peaks of ρ^E, ρ^P, and ρ^I occur earlier and increase in magnitude, particularly with significant changes in p. Consequently, an increase in p appears to inhibit disease spread. This is because a higher transition proportion means more exposed individuals E become presymptomatic individuals P, which leads to a reduction in the number of infectious individuals I (the infection source), thereby suppressing the epidemic.

4.1 Threshold behaviors

In this subsection, we explore how various parameters of system (4) affect epidemic threshold β_c and discuss prevention and control strategies for the influence of parameters. Figure 10 presents an analysis of the effects of the information-diffusion rate λ, infection-rate ratio δ, and transition ratio p on the epidemic threshold β_c for the SF-SF network (the

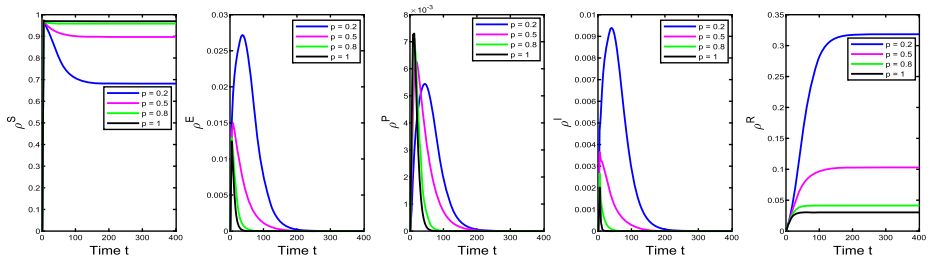

Figure 9 With different transition proportion p, the time evolutions of ρ^S, ρ^E, ρ^P, ρ^I, ρ^R on the SF-SF network

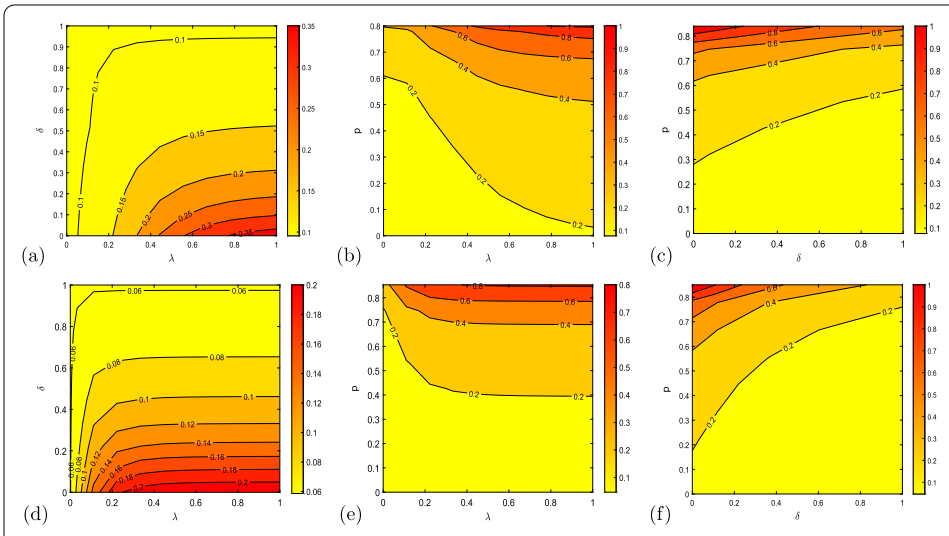

Figure 10 The effects of the information-diffusion rate λ, infection-rate ratio δ, and transition ratio p on the epidemic threshold β_c for the SF-SF network (the first row) and the R-R network (the second row)

first row) and the R-R network (the second row), using contour plots. In Fig. 10(a), with a fixed δ, β_c increases as λ rises. This trend becomes more obvious when $\lambda > 0.2$. These results suggest that higher values of λ and lower values of δ lead to a higher epidemic threshold, which is beneficial for controlling large-scale outbreaks. In Fig. 10(b), with a fixed p, β_c increases as λ increases. Similarly, with a fixed λ, β_c rises as p increases. When both λ and p are large, the increase in β_c is more rapid. This indicates that higher values of λ and p both contribute to raising the epidemic threshold, which helps to suppress the spread of the disease. In Fig. 10(c), an increase in δ lowers the epidemic threshold, while an increase in p has the opposite effect. Thus, lower δ and higher p are beneficial for controlling the disease spread. Figures 10(d) and (e) show similar trends to Figs. 10(a)–(c), but with a lower threshold in random networks compared to scale-free networks, indicating that random networks facilitate disease outbreaks more than scale-free networks. Overall, increasing the information-diffusion rate and transition ratio while decreasing the infection-rate ratio can effectively raise the epidemic threshold and aid in disease-outbreak control.

4.2 Adaptive behavior

After an infectious disease outbreak, individuals often engage in adaptive behaviors, such as wearing masks, avoiding public spaces, or minimizing direct contact with infected in-

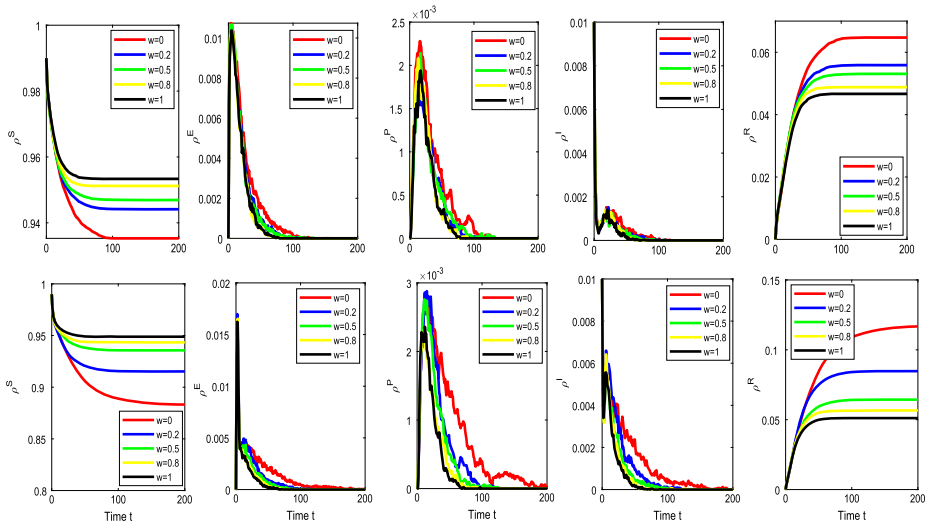

Figure 11 With different rewiring rate w, the time evolutions of ρ^S, ρ^E, ρ^P, ρ^I, ρ^R on the SF-SF network (the first row) and the R-R network (the second row)

dividuals, to reduce their risk of infection upon receiving information about the disease. In this context, we examine how these adaptive behaviors, modeled within the physical contact layer (i.e., the disease-transmission layer) of our two-layer network model, affect the dynamics of disease spread. We analyze how these behavioral adaptations impact the disease spread within this framework.

In the real world, we recognize that susceptible individuals disconnect from infected individuals with a certain probability only after receiving information about the disease. In contrast, those who have not been informed generally do not proactively alter their behavior. Drawing inspiration from the adaptive reconnection mechanism proposed by Gross et al. [39], we then propose an adaptive reconnection mechanism that integrates information diffusion. In this mechanism, the aware and susceptible individuals will disconnect from infected individuals at a rate w and simultaneously establish connections with other noninfected individuals (susceptible individuals S or recovered individuals R) at the same rate w. This mechanism not only reduces the risk of infection transmission but also helps maintain the normal functioning of individuals' social interactions. Given that the adaptive reconnection mechanism of coupled information diffusion has no effect on the information diffusion of the information layer, we only demonstrate its impact on the spread of the disease layer here.

In the first row of Fig. 11, which corresponds to the scale-free network, we observe that as w increases, the rate of ρ^S decrease slows, and its final steady-state value increases. Although the peak values of ρ^E (exposed), ρ^P (prevented), and ρ^I (infected) show a slight decrease, the overall final epidemic size also decreases. In the second row of Fig. 11, which depicts the random network, a similar trend is observed. However, the impact of increasing w is more pronounced compared to the scale-free network, showing a more significant effect on the dynamics of disease spread.

Table 1 Node ranking and influence values across various evaluation methods in the SF-SF network

Number	C_{ncd}	Node	C_{nc}	Number	C_d	Number	C_{kc}
982	36.2702611819695	982	26	109	9	7	4
765	33.9425323245692	765	25	158	9	34	4
350	33.03543667	350	24	177	9	132	4
780	30.28747531	854	23	178	9	146	4
7	30.18069802	432	22	350	9	315	4
293	30.15126129	178	21	432	9	350	4
907	29.94455449	546	21	436	9	520	4
854	29.93692684	780	21	546	9	528	4
609	29.88513388	907	21	637	9	780	4
15	29.6000679	158	20	765	9	907	4
315	29.55312663	177	20	804	9	982	4
742	28.86077093	293	20	854	9	1	3

Table 2 Node ranking and influence values across various evaluation methods in the R-R network

Number	C_{ncd}	Node	C_{nc}	Number	C_d	Number	C_{kc}
356	104.2124293	356	87	356	16	7	7
126	103.2896591	126	86	7	15	127	7
322	98.57667371	322	83	126	15	193	7
852	96.72950686	561	82	322	15	256	7
373	96.30750611	373	81	373	15	296	7
561	96.30348442	852	80	561	15	315	7
862	93.65776048	862	77	576	15	339	7
811	93.16825095	864	77	707	15	351	7
864	92.98705289	909	76	16	14	356	7
622	91.64300491	622	75	677	14	419	7
909	91.52642693	811	75	738	14	433	7
315	91.12183607	306	74	852	14	555	7

4.3 Analysis of node influence

In this subsection, we utilize four evaluation methods including degree centrality C_d [40], K-core centrality C_{kc} [41], neighborhood core centrality C_{nc} [42], and neighborhood core diversity centrality C_{ncd} to rank node influence in SF-SF and R-R networks. The numbers of the top 12 nodes by influence for each method are listed in Table 1 and Table 2. As observed from these tables, the rankings produced by the first three methods differ significantly from each other. In contrast, the fourth method shows some same numbers as the third method.

5 Conclusions and discussions

In this paper, we develop a two-layered network propagation dynamic model to capture the early stages of the COVID-19 outbreak, before control measures were implemented, and to account for the diffusion of disease-related information on online social networks. The upper layer represents information diffusion using the UAU model, while the lower layer models disease dynamics with the SEPIR model. We assume that aware and susceptible individuals, who take preventive measures like reducing public activities, maintaining social distancing, and paying attention to personal hygiene, are infected at a rate δ times lower than unaware and susceptible individuals, where $0 \leq \delta \leq 1$. Furthermore, once unaware and exposed individuals (UE) transition to the unaware and infected individuals (UA), they will immediately actively acquire disease information and transition into an aware and infected individual (AI), thus the UA state is excluded from the model.

Once an unaware and susceptible individual is infected, they immediately acquire disease information and transition to the aware and infected state (AI), thus the UA state is excluded from the model.

Utilizing the micro-Markov-chain approach, we constructed a UAU–$SEPIR$ model comprising nine coupling states. Our analysis reveals that the epidemic threshold β_c of the disease layer is influenced by the information diffusion dynamics and the disease layer's network topology. Additionally, the proportion $1-p$ of exposed individuals who progress to the infected state and the recovery rate r_2 from the infected to the recovered state also significantly impact β_c.

We validate the rationality of the UAU–$SEPIR$ propagation dynamics model (4) through random simulations, and further study the interaction between information diffusion and infectious-disease spread across four two-layered network types: SF-SF, R-R, SF-R, and R-SF. Our findings reveal: 1) An increased information-diffusion rate λ enhances information diffusion, which in turn suppresses disease transmission. Disease spread is more sensitive to network-structure changes; 2) An increased infection rate β accelerates disease spread, leading to an earlier peak and higher peak value, thereby increasing the epidemic size, although the effect diminishes when $\beta > 0.5$. Scale-free network structures in the disease layer tend to reduce the final epidemic size; 3) A higher individual forgetting rate γ significantly impedes information diffusion but accelerates disease spread, increasing the high peak value of infection. The final epidemic sizes follow the order: R-SF<SF-SF<R-R<SF-R; 4) A higher infection-rate ratio δ accelerates disease spread, whereas a larger transition proportion p inhibits it; 5) A larger information-diffusion rate λ, a larger transition proportion p, and a smaller δ raise the epidemic threshold, making it easier to control a large-scale outbreak of the disease.

In addition, considering that individuals typically engage in adaptive behaviors, such as severing contact with infected individuals upon receiving disease-related information, we incorporated this adaptive behavior into our two-layered network propagation dynamics model. Specifically, aware and susceptible individuals (US) actively disconnect from infected individuals (I) and establish connections with noninfected individuals (S or R). Numerical simulations reveal that, within both scale-free and random networks in the disease layer, an increase in rewiring rate w leads to a reduction in both the high peak value of infection and final epidemic size. This effect is notably more pronounced in random networks, suggesting that adaptive behaviors are more effective at curbing disease spread in such networks.

This paper considers the early stage of the COVID-19 outbreak, focusing on the interaction between information diffusion and disease spread in the two-layered network. As the pandemic progressed, people were influenced by the mass-media coverage of COVID-19 [43–45], leading them to adopt active prevention and control measures, such as home isolation and vaccination. These actions contribute to changes in network structure over time. Consequently, future research can explore the impact of mass media on sudden infectious disease events within the framework of time-varying networks.

Appendix: The time evolution on the densities of various disease states and information states

Figure 12 shows that for both layers of the network, which are random networks, the numerical results align well with the random simulation results. The time evolutions shown

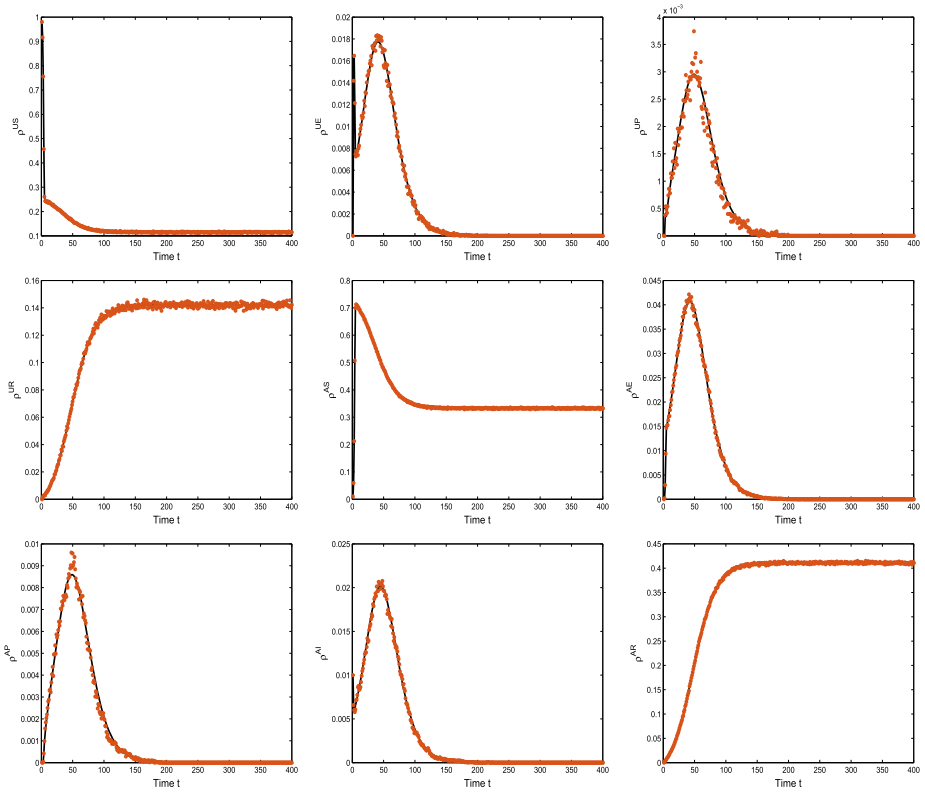

Figure 12 The time evolutions of ρ^{US}, ρ^{AS}, ρ^{UE}, ρ^{AE}, ρ^{UP}, ρ^{AP}, ρ^{AI}, ρ^{UR}, ρ^{AR} in the R-R network. The black curves represent the results from numerical simulations of system (4), while the brown circles indicate the average values obtained from 50 random simulations. Parameters are $\lambda = 0.28$, $\gamma = 0.3$, $\beta = 0.24$, $\delta = 0.2$, $\sigma = 1/7$, $p = 0.2$, $r_1 = 0.14$, $r_2 = 0.33$

in Fig. 12 are basically consistent with the density changes of the corresponding states shown in Fig. 4, hence they will not be repeated here.

Acknowledgements
Not applicable.

Author contributions
LY contributed to modeling, software, writing the original draft, and visualization. ZW contributed to validation, supervision, writing, reviewing, and editing. All the authors read and approved the final manuscript.

Funding
The research was supported by the National Science Fund for Distinguished Young Scholarship of China (No. 62025602).

Data availability
There are no associated data or material in this research work.

Declarations

Competing interests
There are no conflicts of associated interest in this research work.

Author details
[1]School of Computer Science, Northwestern Polytechnical University, Xi'an, 710072, Shaanxi, P.R. China. [2]School of Cybersecurity, Northwestern Polytechnical University, Xi'an, 710072, Shaanxi, P.R. China.

Received: 5 October 2024 Accepted: 4 December 2024 Published online: 19 December 2024

References

1. Flaxman, S., Mishra, S., Gandy, A., et al.: Estimating the effects of non-pharmaceutical interventions on COVID-19 in Europe. Nature **584**(7820), 257–261 (2020)
2. Webster, P.: COVID-19 timeline of events. Nat. Med. **27**(12), 2054–2055 (2021)
3. Haleem, A., Javaid, M., Vaishya, R.: Effects of COVID-19 pandemic in daily life. Curr. Med. Res. Pract. **10**(2), 78 (2020)
4. Wang, Z., Mu, C., Hu, S., Chu, C., Li, X.: Modelling the dynamics of regret minimization in large agent populations: a master equation approach. In: IJCAI–22 pp. 524–540. (2022)
5. Padhan, R., Prabheesh, K.P.: The economics of COVID-19 pandemic: a survey. Econ. Anal. Policy **70**, 220–237 (2021)
6. Chakraborty, I., Maity, P.: COVID-19 outbreak: migration, effects on society, global environment and prevention. Sci. Total Environ. **728**, 138882 (2020)
7. Focosi, D., Novazzi, F., Baj, A., et al.: Monkeypox: an international epidemic. Rev. Med. Virol. **32**(6), e2392 (2020)
8. Zumla, A., Valdoleiros, S.R., Haider, N., et al.: Monkeypox outbreaks outside endemic regions: scientific and social priorities. Lancet Infect. Dis. **22**(7), 929–931 (2022)
9. Kumar, S., Subramaniam, G., Karuppanan, K.: Human monkeypox outbreak in 2022. J. Med. Virol. **95**(1) (2023)
10. Ferdous, J., Barek, M.A., Hossen, M.S., et al.: A review on monkeypox virus outbreak: new challenge for world. Health. Sci. Rep. **6**(1), e1007 (2023)
11. Kermack, W.O., McKendrick, A.G.: A contribution to the mathematical theory of epidemics. Proc. R. Soc. A **115**, 700–721 (1927)
12. Pastor-Satorras, R., Vespignani, A.: Epidemic spreading in scale-free networks. Phys. Rev. Lett. **86**(14), 3200 (2001)
13. Newman, M.E.J.: Threshold effects for two pathogens spreading on a network. Phys. Rev. Lett. **95**(10), 108701 (2005)
14. Moreno, Y., Pastor-Satorras, R., Vespignani, A.: Epidemic outbreaks in complex heterogeneous networks. Eur. Phys. J. B **26**(4), 521–529 (2020)
15. Keeling, M.J., Eames, K.: Networks and epidemic models. J. R. Soc. Interface **2**(4), 295–307 (2005)
16. Wang, Z., Jusup, M., Guo, H., et al.: Communicating sentiment and outlook reverses inaction against collective risks. Proc. Natl. Acad. Sci. USA **117**(30), 17650–17655 (2020)
17. Bauch, C.T.: The spread of infectious diseases in spatially structured populations: an invasory pair approximation. Math. Biosci. **198**(2), 217–237 (2005)
18. Li, J., Jin, Z., Yuan, Y., Sun, G.Q.: A non-Markovian SIR network model with fixed infectious period and preventive rewiring. Comput. Math. Appl. **75**(11), 3884–3902 (2018)
19. Feng, S., Zhang, J., Li, J., et al.: The impact of quarantine and medical resources on the control of COVID-19 in Wuhan based on a household model. Bull. Math. Biol. **84**(4), 47 (2022)
20. Cencetti, G., Contreras, D.A., Mancastroppa, M., et al.: Distinguishing simple and complex contagion processes on networks. Phys. Rev. Lett. **130**(24), 247401 (2023)
21. Daley, D.J., Kendall, D.G.: Epidemics and rumours. Nature **204**(4963), 1118 (1964)
22. Xu, Q., Su, Z., Zhang, K., et al.: Epidemic information dissemination in mobile social networks with opportunistic links. IEEE T. Emerg. Top. Com. **3**(3), 399–409 (2015)
23. Matsubara, Y., Sakurai, Y., Prakash, B.A., et al.: Nonlinear dynamics of information diffusion in social networks. ACM Trans. Web **11**(2), 1–40 (2017)
24. Guo, H., Mu, C., Chen, Y., Shen, C., Hu, S., Wang, Z.: Multi-Agent, Human-Agent and Beyond: a Survey on Cooperation in Social Dilemmas. Neurocomputing **12851** (2024)
25. Wang, X., Zhu, X., Tao, X., et al.: Anomalous role of information diffusion in epidemic spreading. Phys. Rev. Res. **3**(1), 013157 (2021)
26. Dinh, L., Parulian, N.: COVID-19 pandemic and information diffusion analysis on Twitter. Proc. Assoc. Inf. Sci. Technol. **57**(1), e252 (2020)
27. Bauch, C.T., Galvani, A.P.: Social factors in epidemiology. Science **342**(6154), 47–49 (2013)
28. Granell, C., Gómez, S., Arenas, A.: Dynamical interplay between awareness and epidemic spreading in multiplex networks. Phys. Rev. Lett. **111**(12), 128701 (2013)
29. Zheng, C., Wang, Z., Xia, C.: A novel epidemic model coupling the infectious disease with awareness diffusion on multiplex networks. CCDC. **3824**(3830) (2018)
30. Wang, Z., Jusup, M., Wang, R.W., Shi, L., Iwasa, Y., Moreno, Y., Kurths, J.: Onymity promotes cooperation in social dilemma experiments. Sci. Adv. **3**(3), e1601444 (2017)
31. Guo, Q., Jiang, X., Lei, Y., et al.: Two-stage effects of awareness cascade on epidemic spreading in multiplex networks. Phys. Rev. E **91**(1), 012822 (2015)
32. Wang, Z.S., Guo, Q.T., et al.: The impact of awareness diffusion on SIR-like epidemics in multiplex networks. Appl. Math. Comput. **349**(5), 134–147 (2019)
33. Wang, Z., Jusup, M., Shi, L., Lee, J.H., Iwasa, Y., Boccaletti, S.: Exploiting a cognitive bias promotes cooperation in social dilemma experiments. Nat. Commun. **9**(1), 2954 (2018)
34. Juher, D., Saldaña, J.: Tuning the overlap and the cross-layer correlations in two-layer networks: application to a susceptible-infectious-recovered model with awareness dissemination. Phys. Rev. E **97**(3), 032303 (2018)
35. Ye, Y., et al.: Effect of heterogeneous risk perception on information diffusion, behavior change, and disease transmission. Phys. Rev. E **102**(4), 042314 (2020)
36. Chen, J., Hu, M., Cao, J.: Dynamics of information-awareness-epidemic-activity coevolution in multiplex networks. Phys. Rev. Res. **5**(3), 033065 (2023)
37. Feng, M., Li, X., Li, Y., et al.: The impact of nodes of information dissemination on epidemic spreading in dynamic multiplex networks. Chaos. **33**(4) (2023)
38. Tang, B., et al.: Estimation of the transmission risk of the 2019-nCoV and its implication for public health interventions. J. Clin. Med. **462** (2020)
39. Gross, T., D'Lima, C.J., Blasius, B.: Epidemic dynamics on an adaptive network. Phys. Rev. Lett. **96**(20), 208701 (2006)
40. Freeman, L.C.: Centrality in social networks conceptual clarification. Soc. Networks (1978)
41. Kitsak, M., et al.: Identification of influential spreaders in complex networks. Nat. Phys. **6**(11), 888–893 (2010)
42. Bae, J., Sangwook, K.: Identifying and ranking influential spreaders in complex networks by neighborhood coreness. Phys. A **395**, 549–559 (2014)

43. Anwar, A., Malik, M., Raees, V., et al.: Role of mass media and public health communications in the COVID-19 pandemic. Cureus. **12**(9) (2020)
44. Arriaga, P., Esteves, F., Pavlova, M.A., et al.: Coronavirus disease (COVID-19): the impact and role of mass media during the pandemic. Front. Psychol. **12**, 729238 (2021)
45. Koutou, O., Sangaré, B.: Mathematical analysis of the impact of the media coverage in mitigating the outbreak of COVID-19. Math. Comput. **205**, 600–618 (2023)

Publisher's Note